LAWRENCE
LIVERMORE
NATIONAL
LABORATORY

LLNL-JRNL-658686

Accurate Local Event Locations in Rock Valley Nevada Using a Bayesian Multiple Event Method

M. L. Pyle, S. C. Myers, W. R. Walter, K. D. Smith

August 12, 2014

Bulletin of the Seismological Society of America

Disclaimer

This document was prepared as an account of work sponsored by an agency of the United States government. Neither the United States government nor Lawrence Livermore National Security, LLC, nor any of their employees makes any warranty, expressed or implied, or assumes any legal liability or responsibility for the accuracy, completeness, or usefulness of any information, apparatus, product, or process disclosed, or represents that its use would not infringe privately owned rights. Reference herein to any specific commercial product, process, or service by trade name, trademark, manufacturer, or otherwise does not necessarily constitute or imply its endorsement, recommendation, or favoring by the United States government or Lawrence Livermore National Security, LLC. The views and opinions of authors expressed herein do not necessarily state or reflect those of the United States government or Lawrence Livermore National Security, LLC, and shall not be used for advertising or product endorsement purposes.

Accurate Local Event Locations in Rock Valley Nevada Using a Bayesian Multiple Event Method

Moira L. Pyle[1], Stephen C. Myers[2], William R. Walter[3], and Kenneth D. Smith[4]

[1]Lawrence Livermore National Laboratory

7000 East Ave.

Livermore, CA 94550

pyle4@llnl.gov

925-423-3820

[2,3]Lawrence Livermore National Laboratory, Livermore, CA 94550, USA

[4]The Nevada Seismological Laboratory, University of Nevada-Reno, Reno, NV 89557, USA

Prepared for submission to BSSA

LLNL-JRNL-658686

Abstract

The Source Physics Experiment (SPE) is a series of chemical explosions at the Nevada National Security Site (NNSS) designed to improve our understanding of explosion physics. A future SPE will place an explosion at the hypocenter of a small, shallow earthquake, providing a direct earthquake-to-explosion experiment. Candidate earthquakes for this novel experiment come from a sequence of over 200 unusually shallow events that occurred in Rock Valley, Nevada in the southeastern portion of the NNSS during 1993. We apply the Bayesloc multiple-event location algorithm (Myers *et al.*, 2007; 2009) to determine the best possible locations and depths for these events. Past nuclear tests in the nearby Yucca Flat on the NNSS are relocated with the same method to provide insight into the accuracy and uncertainties associated with the Bayesloc location results for the Rock Valley earthquakes. This test suggests that we can accurately pinpoint the location of the Rock Valley events within approximately 1 km of their true locations using direct arrival times only. The incorporation of differential arrival times and a potential ground truth event can significantly decrease the already small uncertainties associated with the epicenter locations. Depth determinations have uncertainties of a few kilometers. Depth uncertainty may be reduced by developing an accurate 3-dimesional model of P-wave and S-wave velocity for Rock Valley.

Introduction

The science of nuclear test monitoring relies on seismic methods to distinguish between earthquake and explosion sources. Unfortunately, the physics behind the differences in observed seismic recordings of the different source types remains incompletely understood. The Source Physics Experiment (SPE) series is a long-term effort designed to advance seismic monitoring through better understanding of explosion physics and associated simulation codes (Snelson *et al.*, 2013). The primary component of the SPE involves the detonation, recording, and modeling of chemical explosions of varying size and depth of burial. The first phase of the experiment is being conducted in the Climax Stock granite at the Nevada National Security Site (NNSS), northwest of Las Vegas. A second phase will take place in a different geology; the alluvium in the Yucca Flat of the NNSS, and a third phase is planned to be a direct earthquake-to-explosion comparison in Rock Valley at the southeastern portion of the NNSS (Walter *et al.*, 2012). The locations of the SPE phases as well as historic tests and past natural earthquake seismicity are shown in Figure 1.

The idea behind the direct earthquake-to-explosion comparison is to drill to the hypocenter of a small, shallow earthquake and detonate an explosion that will be recorded at a common set of receivers. The co-location of sources and sensors eliminates the depth and material property differences of the two different source types and allows for a better investigation of the source mechanism and spectra differences. This possibility arises from an area of unusually shallow seismicity along the Rock Valley fault system (Figure 1). In the spring of 1993 a series of more than 200 earthquakes along the central portion of the fault was recorded by the local, short-period, Southern Great Basin Seismic Network operated by the University of Nevada-Reno (UNR). Initial examination of these earthquakes suggests that they occurred

mostly at depths between 1.5 and 2.5 km (Shields, 1999), and the sequence provides several candidates for this third phase of the SPE.

The Rock Valley fault system strikes east-northeast and extends 19 km along its central section (Yount *et al.*, 1987) and up to 65 km if portions extending to Frenchman's Flat in the northeast and Amargosa Desert in the southwest are included (Piety, 1996). The dip is 70° southeast in the central part of the fault (Swadley and Huckins, 1990) and displacement along the fault is primarily left-lateral strike-slip (Yount *et al.*, 1987). The geology in Rock Valley is similar to that of the nearby Yucca Flat (Wagoner, 2014) and is comprised of quaternary sediments underlain by Miocene and Oligocene sedimentary rocks lying unconformably on Paleozoic limestone and dolomite units (O'Leary, 2000; Sargent and Stewart, 1971).

The main shock of the 1993 Rock Valley sequence occurred on May 30 with an Mw of 3.8, and at least 10 aftershocks had magnitudes above 2.0 (Shields, 1999). In response to the initiation of the sequence, UNR deployed two additional three-component stations, placing one directly over the main area of seismic activity. As part of a feasibility study for this direct earthquake-to-explosion experiment, we are working to improve our understanding of the region and the propagation of energy from Rock Valley sources to local and regional stations in the western U.S. Eight new seismic stations, including two borehole sensors, some located at the original 1993 sites and some at additional sites, have been installed and ongoing seismicity along the fault is currently being recorded (Figure 2).

One of the most important factors for a successful earthquake-to-explosion comparison is to obtain the best possible locations for the Rock Valley earthquakes. Because the earthquakes occurred in a nearby and similar tectonic setting to previous nuclear test sites, we can use the precisely known locations, depths, and times of the nuclear explosions (Springer *et al.*, 2002) as

a ground-truth test case to give us insight into the uncertainties in our results. To determine the locations for both the earthquakes and the explosions, we use the Bayesloc algorithm (Myers *et al.*, 2007; 2009). Bayesloc is a multiple event locator that takes advantage of the precision brought about by simultaneously considering arrival times from many events and stations combined with the utility of Markov Chain Monte Carlo (MCMC) sampling to robustly search the model space.

Data

The 1993 Rock Valley earthquake sequence includes over 200 events and at least 100 have identifiable phase onsets. However, since we are primarily concerned with an event large enough to be recorded at regional distances for the earthquake-to-explosion comparison, we work with the largest 52 events of the sequence. Magnitudes of these events range from 3.8 for the main shock to about 1.75 for the smaller events. At least 10 of the aftershocks had magnitudes above 2.0 (Shields, 1999). The sequence was well recorded by the Southern Great Basin Seismic Network, as well as two temporary, three-component, stations deployed by UNR after the initiation of the sequence (Figure 2; Smith *et al.*, 2000). The first temporary station, RTPP, was positioned directly above the main epicentral area and recorded very clear S-wave arrivals, providing excellent P-to-S times (Figure 4). The second temporary station, RHAM, was placed approximately 8 km to the northeast of the main area of seismic activity. Only one of the horizontal components functioned for RHAM, but the station still recorded high quality S-wave arrivals. The network stations were short period, vertical instruments, many of which supplied recordings with good quality S-waves in addition to P-waves. In preparation for the planned SPE explosion, eight instruments have been deployed around the location of the 1993 Rock

Valley sequence. Within the past year, stations RTPP, NSP, and MCY have been installed at their original locations while stations RVEE, RVNE, RVSE, and RVRR are new and provide additional azimuthal coverage. The RTPP and RVEE stations include surface as well as 2 Hz borehole instruments at ~100 m depth (Figure 2).

In addition to the Rock Valley earthquakes, we relocate a set of 53 past nuclear tests in the nearby Yucca Flat as a ground truth experiment. The hypocenters and the origin times of the nuclear events are precisely known (Springer *et al.*, 2002), and the results of their relocation can provide us with insight into the uncertainties and the limitations of the Rock Valley earthquake relocations. We choose the Yucca Flat events because of the relatively similar geology to Rock Valley. A network of stations operated by the U.S. Geological Survey recorded a number of the nuclear tests in the 1980's and early 1990's. We select stations from this network to use in the relocation test that mimic the azimuthal distribution of the Rock Valley network as closely as possible. Figure 3 shows the azimuthal distributions of both the Rock Valley network and the chosen stations from the nuclear-event network (with the nuclear-event network rotated by 87 degrees). We replicate the azimuthal distribution quite well, although the event-to-station distances for the nuclear-event network are larger than that of the Rock Valley network, extending to 180 km for the former and only 70 km for the latter. Importantly, the nuclear-test network lacks the important stations directly above the epicenters.

Data from the nuclear tests unfortunately have a few shortcomings compared to the Rock Valley event data, including clipped amplitudes and numerous timing problems. One of the network's primary purposes at the time was to record clear P-wave arrival onsets from the nuclear tests. For this purpose the instruments had high gain settings, yielding waveforms for almost all events and stations like those in Figure 4c. As a result of this extreme clipping, very

few S-wave arrivals are observable for the nuclear events. The S-wave recordings that are usable occur mostly at distances of 60 km or more from the events and provide little constraint on the depths. Only one explosion, with Mw 2.45, was small enough to escape clipping and provide S-wave picks at most of the stations. Lack of S-wave data and stations directly above the events limits the ability of the nuclear data to improve our understanding of how well constrained our depths estimates for the Rock Valley events are. The nuclear data also suffers from numerous timing errors. A few events exhibit arrival times that occur before the known detonation time of the event, others have arrivals hundreds of seconds late relative to the expected arrival time. In most cases, obviously erroneous times are consistent across the entire network of stations, and events with this problem can be used in the relocation test, with the expectation that the resulting origin time estimation of the explosion will be incorrect. We run Bayesloc both with and without the problematic travel times and find no significant difference in the resulting locations.

For both sets of data, an analyst examines and picks all direct arrival times for the first arriving P and S waves. Additionally, we obtain differential arrival times using cross-correlation. We filter the Rock Valley data between 2 and 8 Hz, correlate, and then examine every result with a correlation coefficient above 0.5, discarding results with cycle-skipping or poor waveform matches. The Rock Valley data has a large number of excellent correlations for both P and S-waves (Figure 4b), but the prevalent clipping severely limits the usable correlations for the nuclear data. Cycle skipping occurs frequently. Because we do not filter the clipped data due to complications from frequency-domain artifacts, differences in frequency content often cause the waveform onset to be misaligned in favor of aligning the later, clipped, portion of the waveform (Figure 4e). Despite the occurrence of cycle skipping or onset misalignment

errors, waveforms frequently have high correlation coefficients. To ensure the use of only high quality differential arrival times, we require a correlation coefficient of 0.9 or higher to be included in the relocation analysis. At this threshold we are able to eliminate most of the cycle-skipping and misalignment errors. This restriction severely limits the number of usable differential arrival time measurements. We end up with 1655 direct arrivals for the Rock Valley events and a comparable 1326 arrivals for the nuclear events. Contrastingly, for the differential arrival times, the Rock Valley events provide 10 times the amount of data as the nuclear events, with 6101 usable measurements for the former and only 629 for the latter. The various shortcomings of the nuclear event recordings limit their ability to inform the uncertainties resulting from the higher-quality Rock Valley data, but they still provide an interesting and unique data set that sheds some light on the location problem.

Method

We use the Bayesloc algorithm of Myers *et al.* (2007; 2009) to locate the nuclear tests and Rock Valley earthquakes separately. We provide a brief description of the method here, but for full details the reader should refer to the original papers. Bayesloc approaches the location problem as a hierarchy with three model components: the travel time model, the arrival time model, and the prior model. Each model component is treated as a conditional probability that can be combined into a joint posterior distribution using Bayes' theorem. Bayesloc generates realizations of the various model parameters from the joint posterior distribution using MCMC sampling. The specific sampling algorithms used at each step are described in Myers *et al.* (2007).

The model parameters are based upon the decomposition of an observed arrival time, a_{ijk}, for phase k, from event i, at station j, into the origin time, o_i, the model-predicted arrival time, F_{ijk}, corrections to the model-predicted travel time, δ_{ijk}, and some additional error, e_{ijk}:

$$a_{ijk} = o_i + F_{ijk} + \delta_{ijk} + e_{ijk}.$$

The travel time model allows for corrections to the initial travel time curve:

$$\delta_{ijk} = \alpha_k + \alpha_i + \alpha_j + \alpha_{ik} + \alpha_{jk} + \beta_k G_{ij},$$

where the α*'s* are parameters that shift the travel time curve (F_{ijk}), β_k is a scaling parameter, and G_{ij} is the event-to-station distance. The prior distributions on shift and scaling parameters are assumed to be distributed in a Gaussian manner about F with zero mean and a variance provided by the user (typically chosen to be non-informative), but the posteriori distribution is data driven and non-parametric. For our data sets, we find that only the phase shifts (α_k) are well-resolved and use this as our only travel time curve shift. The arrival time model accounts for errors in the measured arrival time after travel time corrections have been applied (due to picking error or small-scale, path-dependent travel time variations, for example):

$$\varepsilon_{ijk} = a_{ijk} - (o_i + F_{ijk} + \delta_{ijk}).$$

Apriori arrival time errors are assumed Gaussian with zero mean and variance determined by a precision (1/variance) term that can be factored into a number of elements including phase, station, and event precisions. Like travel-time corrections, posteriori arrival time errors are data driven and non-parametric. Each precision factor is modeled as a gamma distribution, and has the effect of up-weighting data that has low variance and down-weighting data with higher variance. As for the travel time model, we find that only the arrival time error phase precision factor is resolved well enough to use for our dataset. To account for mislabeled or erroneous picks, Bayesloc incorporates stochastic phase labels (W_{ijk}) to account for phase misidentification

by the analyst. A prior constraint on the phase label can be enforced and the posteriori phase label probability can be distributed over any one of the phases under consideration or as an outlier. Finally, the origin prior model allows the user to provide constraints for the epicenter, depth, or origin time for any of the events that may be known. In our case, we place a loose prior with a variance of 50 km on the epicenters to prevent sampling from locations outside of the array.

Our work also experiments with the incorporation of differential arrival times, although this addition to Bayesloc is still under development (Myers and Johannesson, 2012). The differential arrival times are modeled in a similar way to direct arrivals:

$$d_{i_1 i_2 jk} = D_{i_1 i_2 jk} - \left[\left(o_{i_1} - o_{i_2}\right) + \left(T_{i_1 jk} - T_{i_2 jk}\right)\right] + e_{i_1 i_2 jk}$$

where d is the measured (from cross-correlation of waveforms) differential travel time, o_{i_1} and o_{i_2} are the origin times of event 1 and event 2, respectively, T is the model-predicted travel time ($T_{ijk} = F_{ijk} + \delta_{ijk}$), and e is some additional error. The apriori additional error is modeled as a Gaussian distribution with a mean at the model predicted differential travel time (after travel time corrections have been applied) and variance determined by a precision factor; posteriori distributions are again data driven and non-parametric. Work is still underway to determine a more optimal sampling method for the joint posterior distribution including differential times, but we include results from the current method in our discussion because it sheds some light on how well we can currently locate these events.

Results and Discussion

Direct Arrival-Times

We begin by relocating the nuclear events using direct arrivals only. We run 10 MCMC chains for 10,000 iterations with the first 50% of the iterations used as a 'burn-in' period to reduce the influence of starting values with little prior information. Our starting velocity model, the LLNL model, was developed for the NNSS using data from nuclear tests recorded at regional stations (Anderson and Myers, 2010) and is shown in Figure 5. Travel time curves are calculated from the velocity model using the TauP toolkit (Crotwell *et al.*, 1999). Bayesloc corrections to the travel time curve are small; mean phase shifts (α's) have values of 0.08 s and -0.07 s, and mean phase-distance scales (β's) have values of -0.26 (s/deg) and 1.28 (s/deg) for P and S, respectively. The adjusted travel time curve at 0 km depth is plotted in Figure 6c along with the event-to-station travel time. P-waves exhibit the most consistent distribution of arrival times and are given the heaviest weight in the arrival time model with a mean value of 13.92, while S arrivals have a mean weight of only 0.31, reflecting the relative inconsistency of the arrival times and their extremely minor contribution to the result. The mean event locations are shown in Figure 6a relative to their known true locations. All of the location results are within 1.7 km of the true epicenters, with an average mislocation of 0.7 km. In almost all cases the true epicenter falls within the cloud of samples from the posterior distributions (like those in Figure 7, for example) that, on average, have sample standard deviations in the north and east directions roughly consistent with 95% confidence at a 1.2 km radius from the estimated epicenter, although individual distributions vary from event to event.

Due to the lack of secondary arrival time measurements in the nuclear dataset, depths for almost all events are very poorly constrained. The true depths for the nuclear tests are all less than 1 km from the surface, and Figure 6b illustrates the large inaccuracies for the mean depth in the Bayesloc results stemming from the large uncertainties for the depth parameter. The trade-

offs between event depth, origin time, and travel time corrections means that, without additional information, the depths are generally not constrained any better than the vague distribution set in the prior model. If we place tight constraints around the known shallow depths in the prior model, as expected, the depth accuracies improve, but the priors do not significantly change the estimation of the epicenter locations. The single explosion for which there is S-wave arrival time data at most of the local stations has the best depth result, with a mislocation of about 1.4 km. The posterior distribution for this event covers about the same sized area for the epicenter location as for events without S-wave measurements, but the range in depth is much smaller (Figure 7).

Although the Bayesloc algorithm allows for corrections to the initial travel time model, we relocate the events from both datasets with a second velocity model to check the dependency of our location results on the particular model used. The MOONHOF model (Hoffman and Mooney, 1984), developed for southern Nevada, is similar to the LLNL model (Figure 5) with the most substantial difference being lower velocities in the uppermost two kilometers of the earth. The MOONHOF model is 2 km/s slower in the uppermost 1 km for both P and S waves, and transitions abruptly to higher velocities at 1 km while the LLNL model has a slight gradient from 1-2 km. Results for the nuclear tests using the MOONHOF model do not vary from the LLNL velocity model results in any significant manner. Differences in travel time corrections, arrival time phase weights and epicenter locations are all extremely small. Posterior distributions have nearly identical sizes and areas of coverage suggesting small changes in the velocity model are well accounted for in the uncertainty estimates using direct arrivals.

We locate the Rock Valley earthquakes with the same initial parameters and LLNL velocity model as the nuclear tests. The primary difference for the Rock Valley case is that we

use a different phase label for the first arriving P and S waves (P_{local} and S_{local}) at station RTPP, which is located directly above the events (Figure 2), while keeping the same P and S phase labels at the rest of the stations. Because RTPP is so close to the events, it is likely that the arriving raypaths are upgoing, as opposed to paths to the rest of the stations that turn deeper in the crust, causing different travel-time correction values for local and more distant phases (e.g. P_{local} and P). The mean travel time curve corrections are again small in all cases (α values of -0.03 s, -0.04 s, -0.05 s, and 0.15 s and β values of 0.59 s/deg, 0.89 s/deg, 1.99 s/deg, and 1.98 s/deg for P_{local}, P, S_{local}, and S, respectively). The corrected travel time curve fit to the arrival time data is shown in Figure 8c. The local phases at RTPP are most precisely fit and given the heaviest weight, with average values of 192.24 and 122.29 for P_{local} and S_{local}, respectively. These values are more than 5 times larger than P and 17 times larger than S (with mean values of 37.11 and 7.24), indicating the importance of the extremely close station in the final results. Event locations are shown in Figure 8, relative to their starting catalog locations, along with a cross-section displaying event depths. The areas covered by epicenter samples from the posterior distributions for the Rock Valley events (shown in Figure 9 for one of the largest aftershocks) are a little bit smaller than those for the nuclear tests, with sample standard deviations that are roughly consistent with 95% confidence in the north and east directions, on average, at a 0.7 km radius from the mean epicenter location. The depth uncertainties reflected by the posterior distributions are much smaller compared to the nuclear tests, due to the station directly above the events and the large number of high-quality S arrival times for Rock Valley.

Relocating the Rock Valley earthquakes using the MOONHOF velocity model returns similar results to those using the LLNL model. Phase weights, average travel time curve corrections, epicenter locations, and posterior distribution coverage areas change very little with

velocity model. The biggest discrepancy between hypocenter parameters determined using the two velocity models is depth. Mean depth values produced using the MOONHOF velocity model are almost universally shallower than depth values using the LLNL model. Average uncertainties, indicated by the posterior distributions, are larger with the MOONHOF model; in general, the samples overlap the area covered by the LLNL model distributions, and expand further into more shallow depths. These results indicate that confidence in depth estimates and uncertainties depends upon confidence in the velocity model.

Differential Arrival-Times

We additionally relocate the Rock Valley events with differential arrival times incorporated into the dataset. Because the sampling for the differential arrivals is still under development, we attempt to ensure the model space is thoroughly explored with a higher volume of sampling than is typically needed for Bayesloc. While for the direct arrival only case we run 10 MCMC chains, here we run 200 chains for 10,000 iterations and again the first 50% are used as a 'burn-in' period. Figure 10 displays the locations resulting from the combination of direct and differential arrivals compared to those using direct arrivals alone. Example posterior distributions for one of the largest aftershocks from both cases are plotted together in Figure 11. In all cases the size of the distribution shrinks dramatically using the direct and differential arrival dataset, but remains within the area covered by the direct arrival only distribution. This suggests that the addition of differential arrival times may be able to reduce the location uncertainties. Figure 10b shows the relocation results with respect to the surface fault trace from Yount *et al.* (1987). The pattern of events does not locate directly on the mapped fault, but we note that it matches well the fault line 0.5-1 km to the north, and this distance is roughly consistent with what would be expected from shallow events along a steeply dipping fault. For

example, simple geometry suggests that for events 0.7 km from the fault along the surface, a fault plane dip of 76° would indicate that the events have a depth of about 3 km while a dip of 45° would indicate a depth of about 1.0 km.

The uncertainty in depth for the Rock Valley events is somewhat improved with the incorporation of the differential arrival time data. Again, we locate the earthquakes with both the LLNL and the MOONHOF velocity models. Figure 11 shows example posterior distributions from both models and Figure 12 contains cross-sections showing the Rock Valley event depths along with the corresponding velocity model for both cases. Epicenter locations from the two velocity models are nearly identical. Although individual posterior distributions suggest that uncertainties in depth are very small, it is apparent from Figure 11 that the distributions resulting from even very small changes to the velocity model do not necessarily overlap. Figure 12 shows that the two similar models can produce differences in event depths of half a kilometer or more on average. These results indicate that the depth uncertainties are underestimated unless the velocity model is correctly known. In order to have an accurate and well-resolved depth estimate, it will be necessary to have an accurate estimate of the seismic velocity for the shallowest geological units of Rock Valley.

The nuclear dataset furnishes a poor direct comparison to the Rock Valley dataset in the differential arrival time case, but the results can be viewed as an upper bound for the location uncertainty in Rock Valley. The small number of usable correlations for the nuclear data (as discussed in the Data section) does not supply much additional constraint to the location problem. Additionally, the nuclear tests occur over a much larger geographical region than Rock Valley, causing higher variability in the few available differential times due to small-scale changes in local structure. However, this limited dataset can be employed to demonstrate the

usefulness of ground truth events in improving the accuracy of the resulting locations. The inclusion of a ground truth event does not impact the epicenter location of even very nearby events when only direct P-wave arrival times from local data are used. When combined with differential arrival time data though, the ground truth event can improve the epicenter location accuracy of events within a few kilometers that have correlations with the ground truth event. Figure 13 displays the results when a subset of the nuclear data, grouped into 3 small clusters, is relocated in a series of cases using differential arrival times and rotating ground truth events. Figure 13a shows the case when no ground truth event is used. When the ground truth event is placed in the westernmost cluster (Figure 13b), which is the most distant from the other two clusters, it improves the epicenter location accuracy within its own cluster, but has little effect on the other two clusters. When the ground truth event occurs in either the southernmost (Figure 13c) or easternmost (Figure 13d) clusters, it results in highly accurate epicenters within its own cluster and improved accuracy in the next closest cluster, but no improvement in the furthest cluster. These results are similar to those of Anderson and Myers (2010), who used absolute time picks. Smaller numbers of correlations between events in the westernmost cluster and those in the other clusters accounts for some of the differences in epicenter accuracy as the ground truth event moves around, but the results suggest that for optimal effect, the ground truth event needs to be situated within 2-3 kilometers of the events it targets to inform. No ground truth event currently exists to aid in the location of the Rock Valley earthquakes, but proposed work would provide us with a known source that could be recorded at a number of the same stations that recorded the Rock Valley sequence.

Conclusions

Relocation of nuclear tests using the Bayesloc algorithm provides us with insight into the uncertainties of our determined locations for the Rock Valley earthquakes of interest to a future SPE direct earthquake-to-explosion comparison experiment. Due to the fact that the nuclear data suffers from a number of shortcomings, most notably clipped amplitudes and a lack of S-wave arrivals, we view the results as an indication of the upper bounds of uncertainties we can expect for the higher quality Rock Valley data. Using a dataset comprised of direct arrival times only, true event epicenters for the nuclear events fall within the cloud of posterior distribution samples from the Bayesloc results, and within 1 km of the mean epicenter in almost all cases. This suggests that the uncertainties of the Rock Valley events, which are slightly smaller than for the nuclear events at 0.7 km on average, are reasonable. Depths for all events, even when S-wave arrivals are present, have larger uncertainty and depend chiefly upon the initial velocity model and whether or not there is a station is within one focal depth of the event. The addition of differential arrival times to the location problem has the potential to further reduce uncertainties in the epicenter location and work is ongoing to assess and improve the incorporation of this kind of data into the Bayesloc method. The inclusion of a ground truth event in the dataset could improve and provide an even greater degree of certainty to the accuracy of the epicenter locations. The resolution of the depths of the events, which is of utmost importance for the proposed SPE project, will require additional refinement of the velocity model in the uppermost few kilometers. These results confirm the unusually shallow nature of Rock Valley Fault Zone seismicity and indicate a clear path forward to achieve the sub-kilometer hypocenter resolution desired for the third phase of SPE. Future work will include a ground-truth explosion within 2 km of the historic Rock Valley sequence to help constrain epicenter resolution, and on-going

noise correlation efforts as well as a planned refraction line will help provide a well-determined local velocity model for better depth control.

Data and Resources

Data used in this study were recorded at seismic stations operated by the U.S. Geological Survey and the University of Nevada-Reno (UNR). Waveform data are stored at the Nevada Seismological Laboratory at UNR, and are publicly available by request. Analysis and graphics software used include SAC (Goldstein *et al.*, 2003), GMT (Wessel and Smith, 1998), and MATLAB.

Acknowledgements

We would like to thank Terri Hauk and Gabe Plank for their assistance with the datasets. The Source Physics Experiments (SPE) would not have been possible without the support of many people from several organizations. The authors wish to express their gratitude to the National Nuclear Security Administration, Defense Nuclear Nonproliferation Research and Development (DNN R&D), and the SPE working group, a multi-institutional and interdisciplinary group of scientists and engineers. This work was done by Lawrence Livermore National Laboratory under award number DE-AC52-07NA27344.

References

Anderson, M. L., and S. C. Myers (2010). Assesment of regional-distance location calibration using a multiple-event location algorithm, *Bull. Seismol. Soc. Am.* **100**, no. 2, 868-875, doi: 10.1785/0120090145.

Crotwell, H. P., T. J. Owens, and J. Ritsema (1999). The TauP Toolkit: Flexible seismic travel-time and ray-path utilities, *Seismol. Res. Lett.* **70**, 154-160.

Goldstein, P., D. Dodge, M. Firpo, and L. Minner (2003). SAC2000: signal processing and analysis tools for seismologists and engineers, invited contribution to the *IASPEI International Handbook of Earthquake and Engineering Seismology*, W. H. K. Lee, H. Kanamori, P. C. Jennings and C. Kisslinger (Editors), Academic Press, London.

Hoffman, L. R., and W.D. Mooney (1984). A seismic study of Yucca Mountain and vicinity, southern Nevada – Data report and preliminary results, *U.S. Geol. Surv. Open-File Rept. 83-588*, 50 pp.

Myers, S. C., G. Johannesson, and W. Hanley (2007). A Bayesian hierarchical method for multiple-event seismic location, *Geophys. J. Int.* **171,** 1049-1063, doi: 10.1111/j.1365-246X.2007.03555.x.

Myers, S. C., G. Johannesson, and W. Hanley (2009). Incorporation of probabilistic seismic phase labels into a Bayesian multiple-event seismic locator, *Geophys. J. Int.* **177,** 193-204, doi: 10.1111/j.1365-246X.2008.04070.x.

Myers, S. C., and G. Johannesson (2012). Extension of the Bayesloc multiple-event location algorithm to include differential travel-time measurements, Proceedings of the *Monitoring Research Review Review, Albuquerque, NM.*

O'Leary, D. W. (2000). Tectonic significance of the Rock Valley Fault Zone, Nevada Test Site, in *Geologic and geophysical characterization studies of Yucca Mountain, Nevada, a potential high-level radioactive-waste repository*, J. W. Whitney and W. R. Keefer (Editors), United States Geologic Survey Data Series: 58.

Piety, L. A. (1996). Compilation of known or suspected Quaternary faults within 100 km of Yucca Mountain, Nevada and California, *U. S. Geol. Surv. Open-File Rept. 94-112*, 404 pp.

Sargent, K. A., and J. H. Stewart, (1971). Geologic map of the Specter Range NW quadrangle, Nye County, Nevada, *U. S. Geol. Surv. Geologic Quadrangle Map GQ-384, scale 1:24,000.*

Shields, G. (1999). Source parameter investigation of the 1993 Rock Valley earthquake sequence, *Masters Thesis*, University of Nevada-Reno, Reno, Nevada.

Smith, K. D., G. Shields, and J. N. Brune (2000). A sequence of very shallow earthquakes in the Rock Valley Fault Zone, Southern Nevada Test Site, in *Geologic and geophysical characterization studies of Yucca Mountain, Nevada, a potential high-level radioactive-waste repository*, J. W. Whitney and W. R. Keefer (Editors), United States Geologic Survey Data Series: 58.

Snelson, C. M., R. E. Abbot, S. T. Broome, R. J. Mellors, H. J. Patton, A. J. Sussman, M. J. Townsend, and W. R. Walter (2013). Chemical explosion experiments to improve nuclear test monitoring, *Eos Trans. AGU* **94**, no. 27, 237-239.

Springer, D. L., G. A. Pawloski, J. L. Ricca, R. F. Rohrer, and D. K. Smith (2002). Seismic source summary for all U. S. below-surface nuclear explosions, *Bull. Seismol. Soc. Am.* **92**, no. 5, 1806-1840.

Swadley, W. C., and H. E. Huckins (1990). Geologic map of the surficial deposits of the Skull Mountain quadrangle, Nye County, Nevada, *U. S. Geol. Surv. Miscellaneous Investigations Series Map 1-1972, scale 1:24,000.*

Walter, W. R., M. L. Pyle, S. R. Ford, S. C. Myers, K. D. Smith, C. Snelson, and V. Chipman (2012). Rock Valley direct earthquake-explosion comparison experiment (RV-DC): Initial feasibility study, Lawrence Livermore National Laboratory Technical Report, *LLNL-TR-585672*, 23 pp.

Wagoner, J. L. (2014). Working toward a site-scale geomodel – Nevada National Security Site, Review of Monitoring Research 17-19 June 2014, Albuquerque, NM

Wessel, P. and W. H. F. Smith (1998). New, improved version of the Generic Mapping Tools released, *EOS Trans. AGU* **79**, 579.

Yount, J. C., R. R. Shroba, C. R. McMasters, H. E. Huckins, and E. A. Rodriguez (1987). Trench logs from a strand of the Rock Valley fault system, Nevada Test Site, Nye County, Nevada, *U.S. Geol. Surv. Miscellaneous Field Studies Map MF-1824*.

List of Figure Captions

Figure 1. Map of the study area. Top right map displays the regional setting. In both maps the thick black outline marks the boundary of the Nevada National Security Site (NNSS). Red stars show locations of past nuclear explosions used in this study and blue stars show locations of events from the 1993 Rock Valley earthquake sequence. Green circle indicates location of SPE phase one, and blue circle indicates location SPE phase two. Heavy black lines through the blue stars show mapped surface locations of the Rock Valley fault (Yount *et al.*, 1987). YM signifies location of Yucca Mountain, SM signifies Skull Mountain, and LSM signifies Little Skull Mountain.

Figure 2. Instrument networks for (a) Nuclear events and (b) Rock Valley events. In both cases blue stars indicate event locations and red triangles indicate stations locations. Solid black outlines mark the boundary of the NNSS. In (b), purple symbols represent stations that are currently operating and also operated in 1993. The light blue symbols indicate new stations. The two circles indicate locations of the borehole stations.

Figure 3. Histograms showing station azimuthal distribution for (a) nuclear-event network and (b) Rock Valley network. Note that the nuclear-event network is rotated by 87 degrees prior to computation of the histogram.

Figure 4. Waveform and correlation examples. (a) Recording at the closest station, RTPP, of one of the large Rock Valley aftershocks. Very clear P and S arrivals are visible. (b) Correlation of two Rock Valley events at station RTPP aligned on the S wave. The Rock Valley data

provided excellent correlations for both P and S waves. (c) Recording at one of the distant stations, GVN of one of the smaller (Mw 3.8) explosions showing the extent of waveform clipping for the nuclear data set. (d) Usable correlation from two clipped nuclear events at station GLR. (e) Poorly aligned correlation from two nuclear events illustrating the potential inaccuracy of differential times based on correlation of clipped data. The two events in this figure are located very close to each other, but likely have differing frequency content due to differences in magnitude (Mw 3.7 and 4.6) causing poor alignment of the P-wave onset, despite a very high correlation coefficient (0.8).

Figure 5. Velocity models used in this study. Solid line indicates the LLNL model from Anderson and Myers (2010), and dotted line indicates the MOONHOF model from Hoffman and Mooney (1984).

Figure 6. Direct arrival location results for nuclear tests using the LLNL velocity model. (a) Map view of epicenter locations. Stars represent the true locations of the nuclear tests and circles denote the Bayesloc locations. Symbol color indicates event depth. Dashed line marks the location of the cross-section plotted in (b). (c) Arrival time data fits to the travel time curve. Red line represents the P-wave corrected travel time curve at 0 km depth and blue line represents the S-wave curve. Black circles and triangles mark P and S arrivals, respectively, calculated using the new event location and origin time, green symbols indicate arrivals calculated from the known locations and origin times. Note that timing errors discussed in the Data section are apparent in some of the travel times calculated using the ground-truth information. Arrivals

from the new locations and origin times show that Bayesloc compensates for these errors with inaccurate origin times, but reasonable locations.

Figure 7. Example posterior distributions for the nuclear tests using the LLNL velocity model and direct arrivals only. In all cases the red star indicates the true location of the event and the blue circle shows the mean of Bayesloc MCMC samples. (a) Map view of the posterior distribution for the one event with S-wave arrival times at most stations. (b) Cross section of posterior distribution for the event in (a). (c) and (d) are the same as (a) and (b) for a different event with no S-wave arrivals.

Figure 8. Direct arrival location results for Rock Valley events using the LLNL velocity model. (a) Map view of epicenter locations. Stars show the starting catalog locations for the events and circles denote the Bayesloc locations. Symbol color indicates event depth. Dashed line marks the location of the cross-section plotted in (b). Red star in (b) represents the main shock and the blue circles represent the largest aftershocks. (c) Arrival time data fits to the travel time curve at 3 km depth. Symbol and line meanings are the same as for Figure 6.

Figure 9. Example posterior distribution for one of the large Rock Valley aftershocks using the LLNL velocity model and direct arrivals only. Similar to Figure 7, except in this case the red star indicates the starting catalog location.

Figure 10. Direct (pick) and differential (cross correlation) arrival time location results for Rock Valley using the LLNL velocity model. (a) Comparison of results using direct arrival data only

(stars) and those using both direct and differential arrival time data (circles). (b) Event locations relative to the Rock Valley fault. Solid black lines mark the mapped fault trace (Yount *et al.*, 1987). The fault dips to the southeast (Swadley and Huckins, 1990) and red lines show the fault traces translated to the south by ~0.7 km, which could be consistent with the location of the fault at depth.

Figure 11. Comparison of posterior distributions for locations of one of the large Rock Valley aftershocks using direct arrival data only and using both direct and differential arrival time data. (a) and (b) show the map view and cross section, respectively for the LLNL velocity model and (c) and (d) show the same for the MOONHOF velocity model. In all cases the red star indicates the starting catalog location. Small dark purple circles show samples from the direct arrival posterior distribution. Large blue circle denotes the mean of the location samples based on direct arrivals. Samples from the differential and direct arrival posterior distribution are represented by small green circles, and the mean of the location samples based on direct and differential arrivals is marked by a large green circle.

Figure 12. Cross sections showing event depths for the Rock Valley earthquakes using (a) the LLNL velocity model and (b) the MOONHOF velocity model. Red star represents the main shock and blue circles represent the largest aftershocks. Error bars indicated two standard deviations. P (red line) and S (blue line) velocity models are also plotted. Distance along the cross section is shown along the top axes while velocity is shown along the bottom axes.

Figure 13. Nuclear test relocation results using differential arrival times and use of a tight location prior on a ground-truth event. In all cases the red stars denote true event locations, black circles show Bayesloc epicenters, and yellow symbols indicate ground-truth events constrained by a tight prior. No priors are used in (a). In cases (b), (c), and (d), a tight prior is used for a different ground-truth event each time to generate the results displayed.

Authors

Moira L. Pyle

Lawrence Livermore National Laboratory

7000 East Ave.

Livermore, CA 94550

pyle4@llnl.gov

925-423-4988

Stephen C. Myers

Lawrence Livermore National Laboratory

7000 East Ave.

Livermore, CA 94550

myers30@llnl.gov

925-423-4988

William R. Walter

Lawrence Livermore National Laboratory

7000 East Ave.

Livermore, CA 94550

walter5@llnl.gov

925-423-8777

Kenneth D. Smith

Nevada Seismological Laboratory
University of Nevada-Reno
MS 174
Reno, NV 89557
ken@seismo.unr.edu
775-784-4218

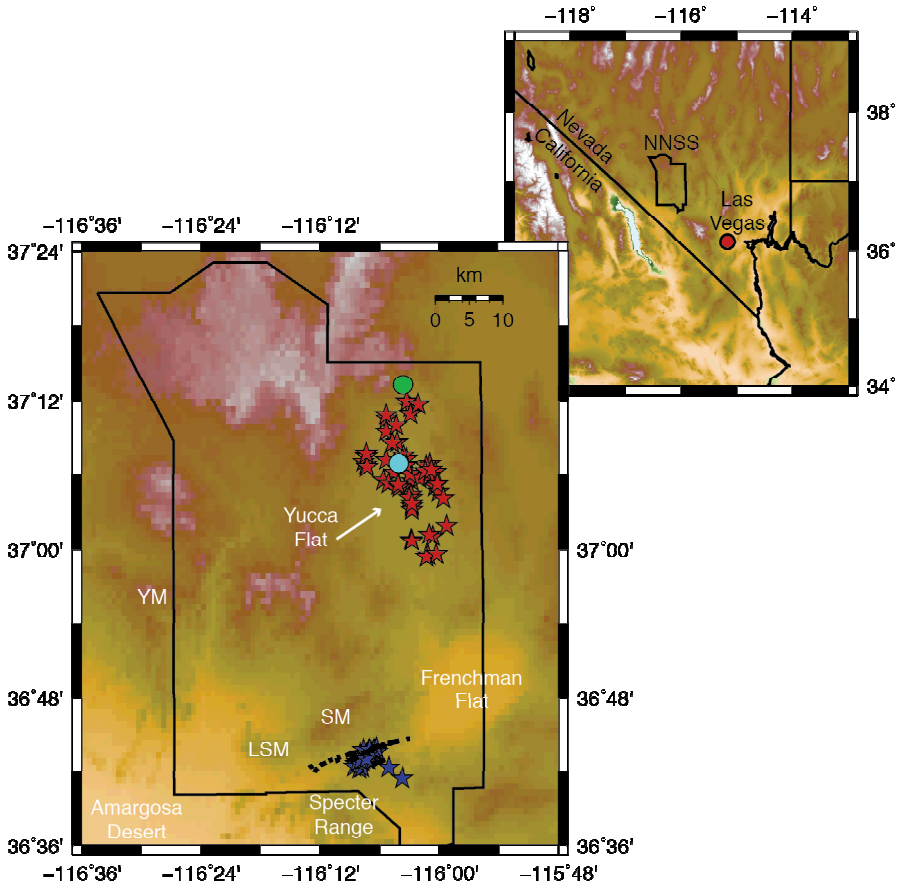

Figure 1. Map of the study area. Top right map displays the regional setting. In both maps the thick black outline marks the boundary of the Nevada National Security Site (NNSS). Red stars show locations of past nuclear explosions used in this study and blue stars show locations of events from the 1993 Rock Valley earthquake sequence. Green circle indicates location of SPE phase one, and blue circle indicates location SPE phase two. Heavy black lines through the blue stars show mapped surface locations of the Rock Valley fault (Yount *et al.*, 1987). YM signifies location of Yucca Mountain, SM signifies Skull Mountain, and LSM signifies Little Skull Mountain.

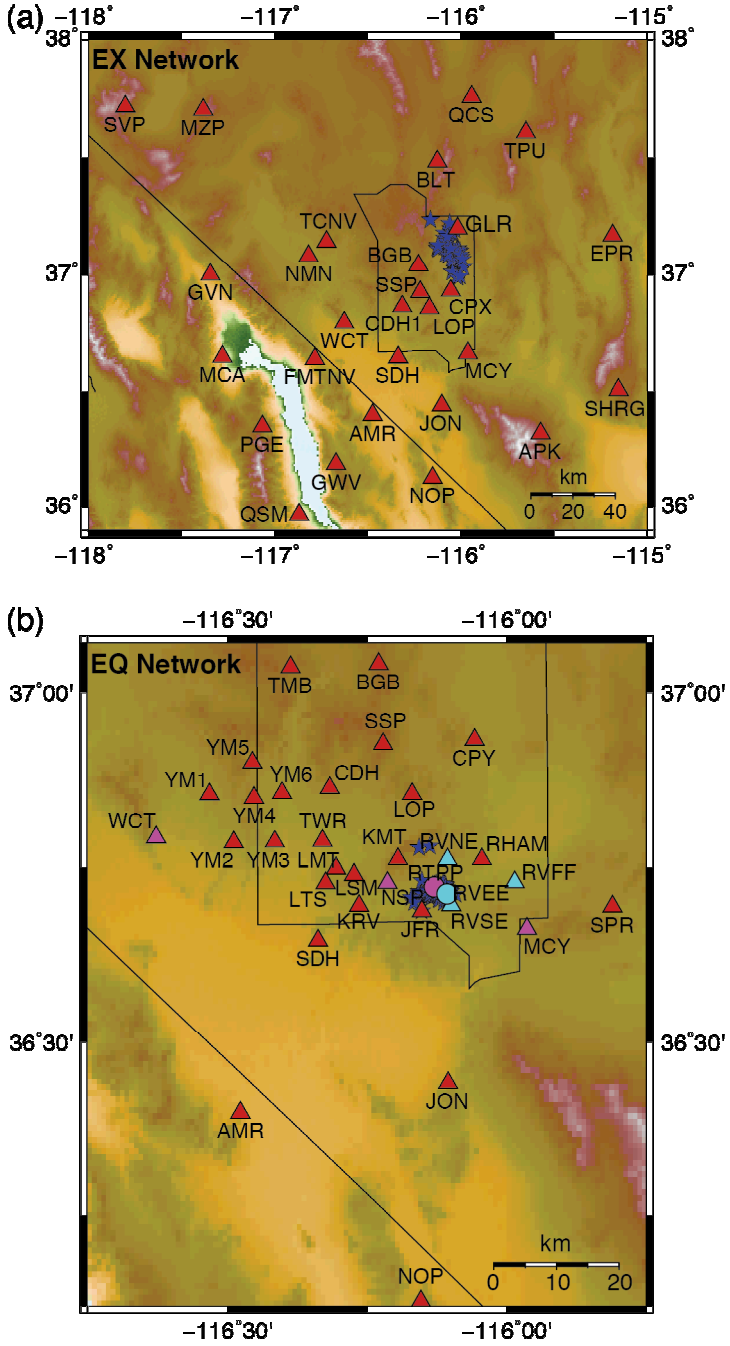

Figure 2. Instrument networks for (a) Nuclear events and (b) Rock Valley events. In both cases blue stars indicate event locations and red triangles indicate stations locations. Solid black outlines mark the boundary of the NNSS. In (b), purple symbols represent stations that are

currently operating and also operated in 1993. The light blue symbols indicate new stations. The two circles indicate locations of the borehole stations.

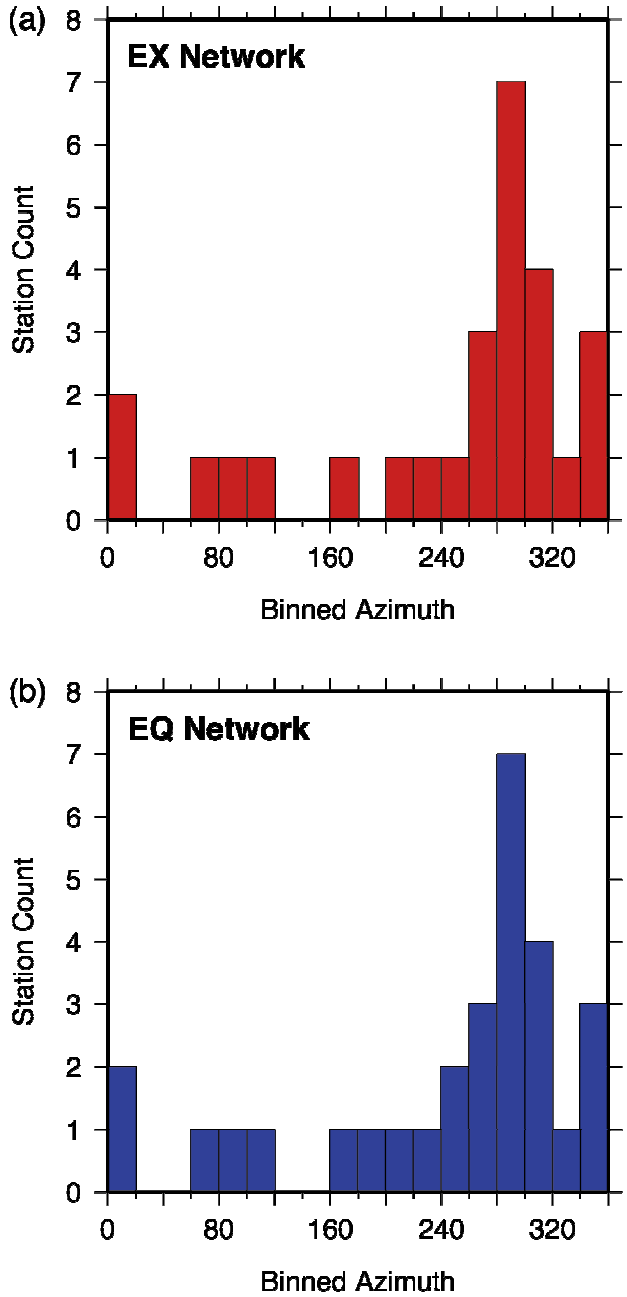

Figure 3. Histograms showing station azimuthal distribution for (a) nuclear-event network and (b) Rock Valley network. Note that the nuclear-event network is rotated by 87 degrees prior to computation of the histogram.

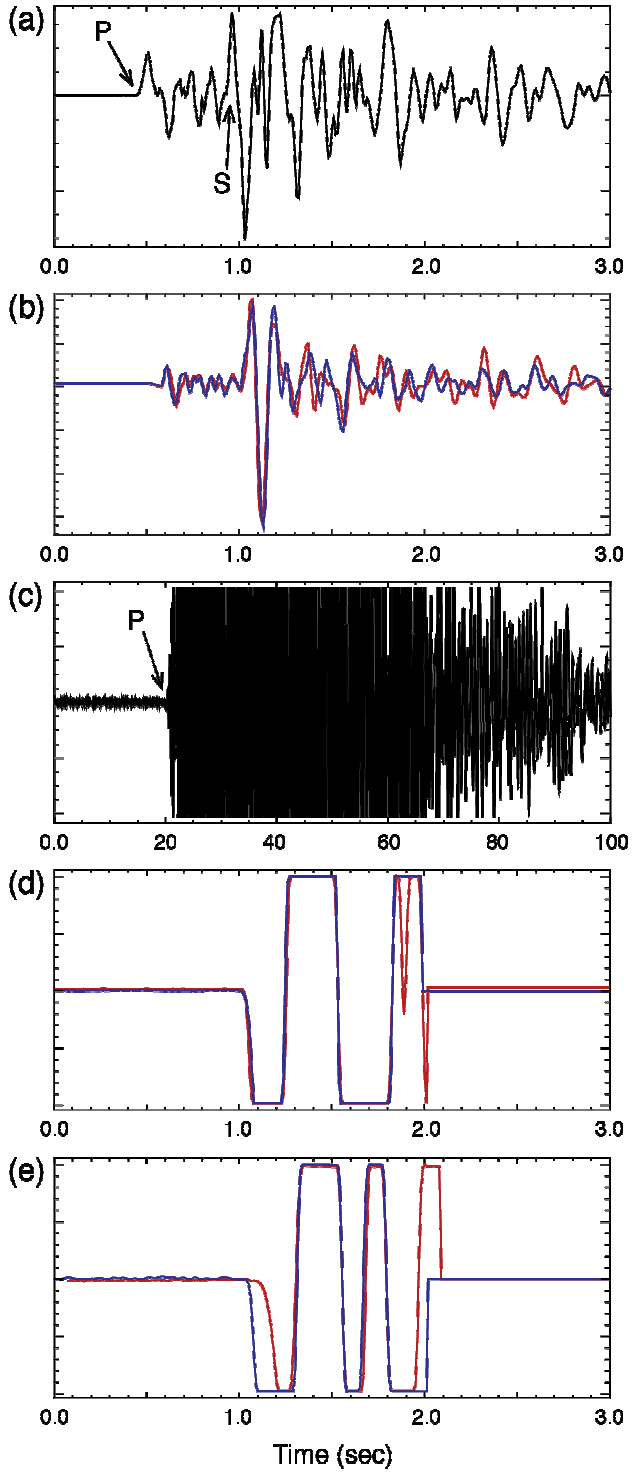
(a)
P
S
0.0
1.0
2.0
3.0
(b)
0.0
1.0
2.0
3.0
(c)
P
0.0
20
40
60
80
100
(d)
0.0
1.0
2.0
3.0
(e)
0.0
1.0
2.0
3.0
Time (sec)

Figure 4. Waveform and correlation examples. (a) Recording at the closest station, RTPP, of one of the large Rock Valley aftershocks. Very clear P and S arrivals are visible. (b) Correlation of two Rock Valley events at station RTPP aligned on the S wave. The Rock Valley data provided excellent correlations for both P and S waves. (c) Recording at one of the distant stations, GVN of one of the smaller (Mw 3.8) explosions showing the extent of waveform clipping for the nuclear data set. (d) Usable correlation from two clipped nuclear events at station GLR. (e) Poorly aligned correlation from two nuclear events illustrating the potential inaccuracy of differential times based on correlation of clipped data. The two events in this figure are located very close to each other, but likely have differing frequency content due to differences in magnitude (Mw 3.7 and 4.6) causing poor alignment of the P-wave onset, despite a very high correlation coefficient (0.8).

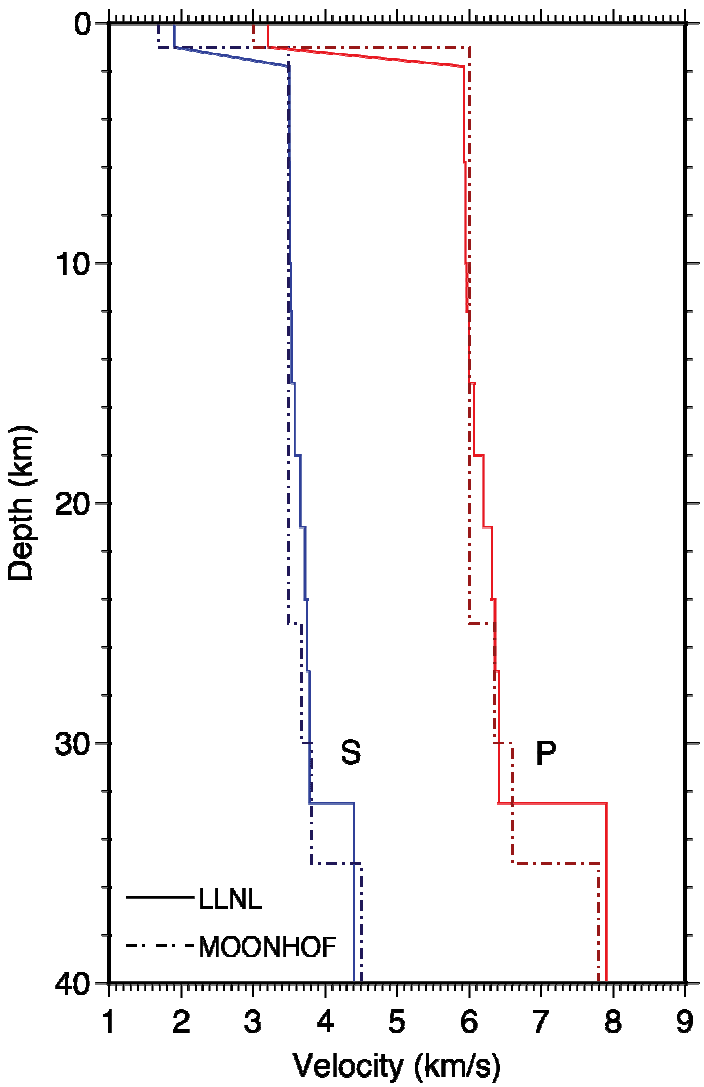

Figure 5. Velocity models used in this study. Solid line indicates the LLNL model from Anderson and Myers (2010), and dotted line indicates the MOONHOF model from Hoffman and Mooney (1984).

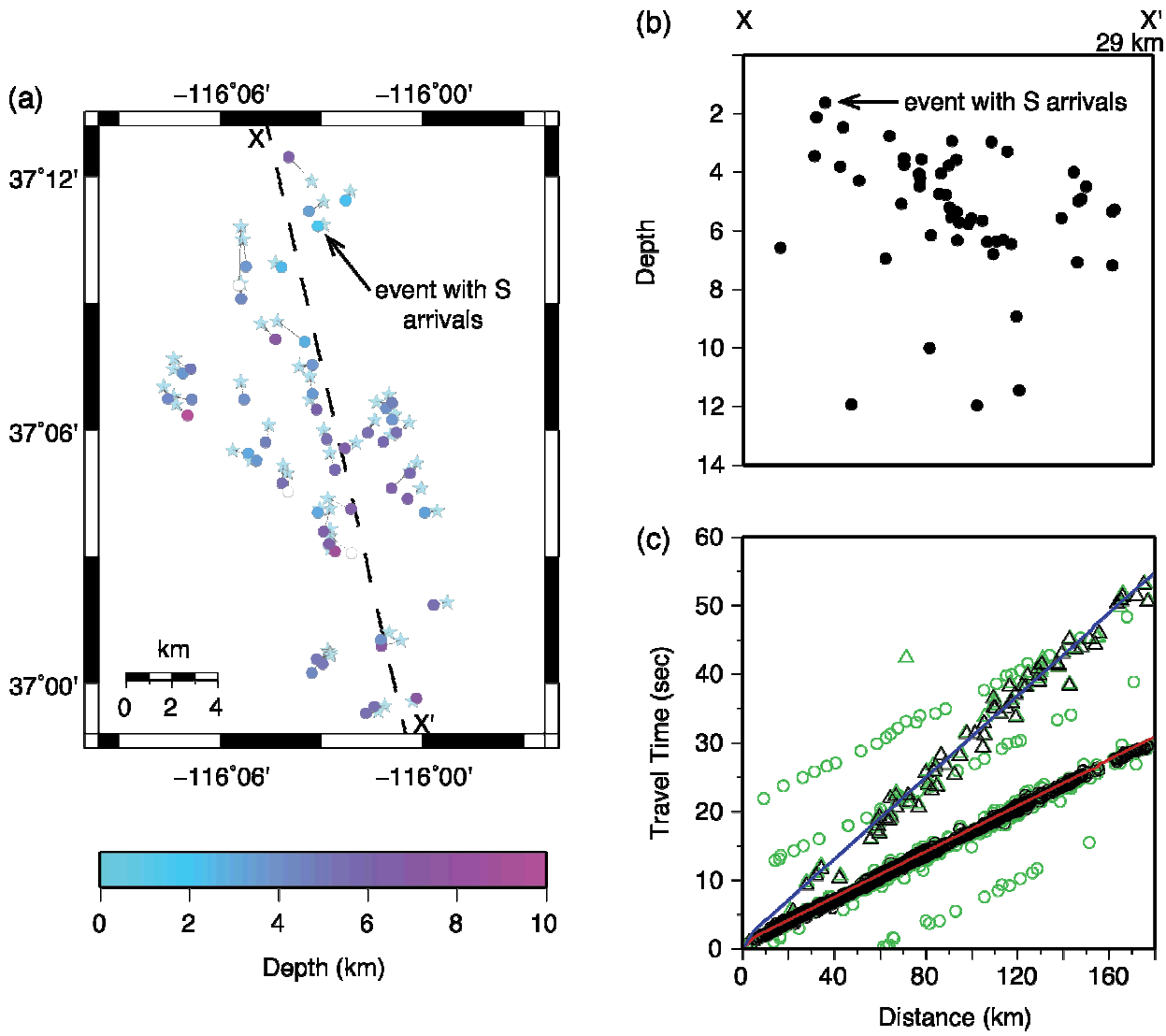

Figure 6. Direct arrival location results for nuclear tests using the LLNL velocity model. (a) Map view of epicenter locations. Stars represent the true locations of the nuclear tests and circles denote the Bayesloc locations. Symbol color indicates event depth. Dashed line marks the location of the cross-section plotted in (b). (c) Arrival time data fits to the travel time curve. Red line represents the P-wave corrected travel time curve at 0 km depth and blue line represents the S-wave curve. Black circles and triangles mark P and S arrivals, respectively, calculated

using the new event location and origin time, green symbols indicate arrivals calculated from the known locations and origin times. Note that timing errors discussed in the Data section are apparent in some of the travel times calculated using the ground-truth information. Arrivals from the new locations and origin times show that Bayesloc compensates for these errors with inaccurate origin times, but reasonable locations.

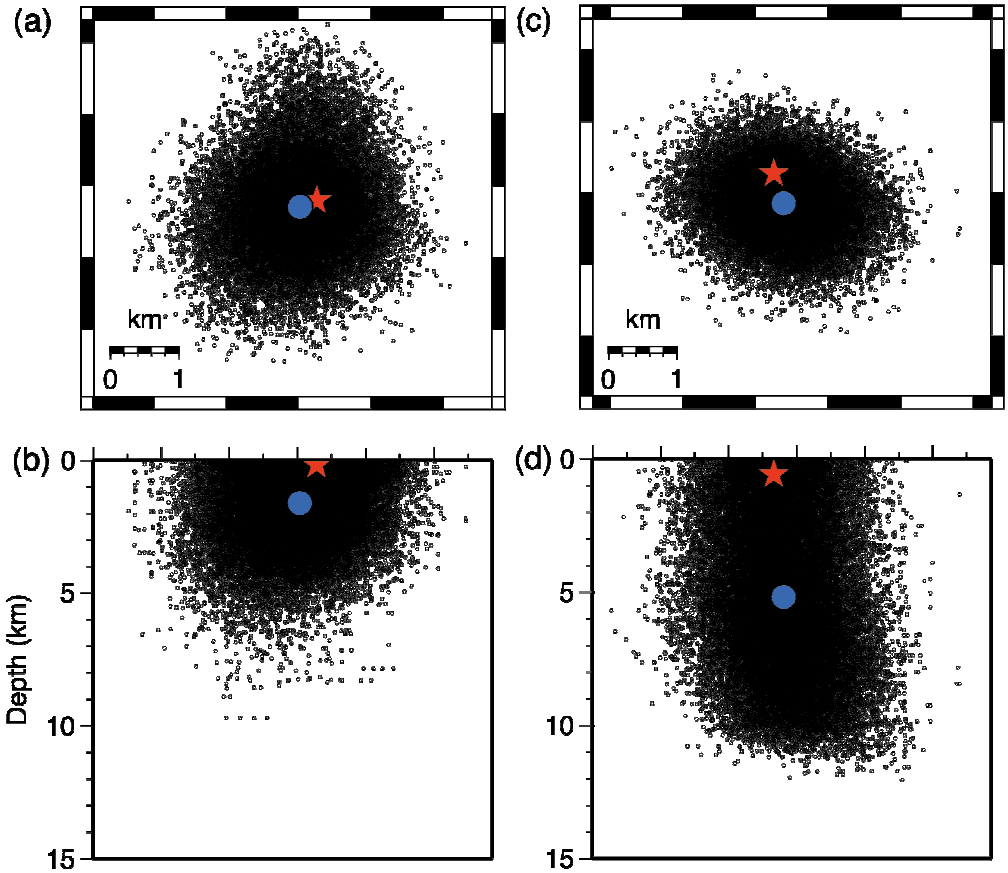

Figure 7. Example posterior distributions for the nuclear tests using the LLNL velocity model and direct arrivals only. In all cases the red star indicates the true location of the event and the blue circle shows the mean of Bayesloc MCMC samples. (a) Map view of the posterior distribution for the one event with S-wave arrival times at most stations. (b) Cross section of posterior distribution for the event in (a). (c) and (d) are the same as (a) and (b) for a different event with no S-wave arrivals.

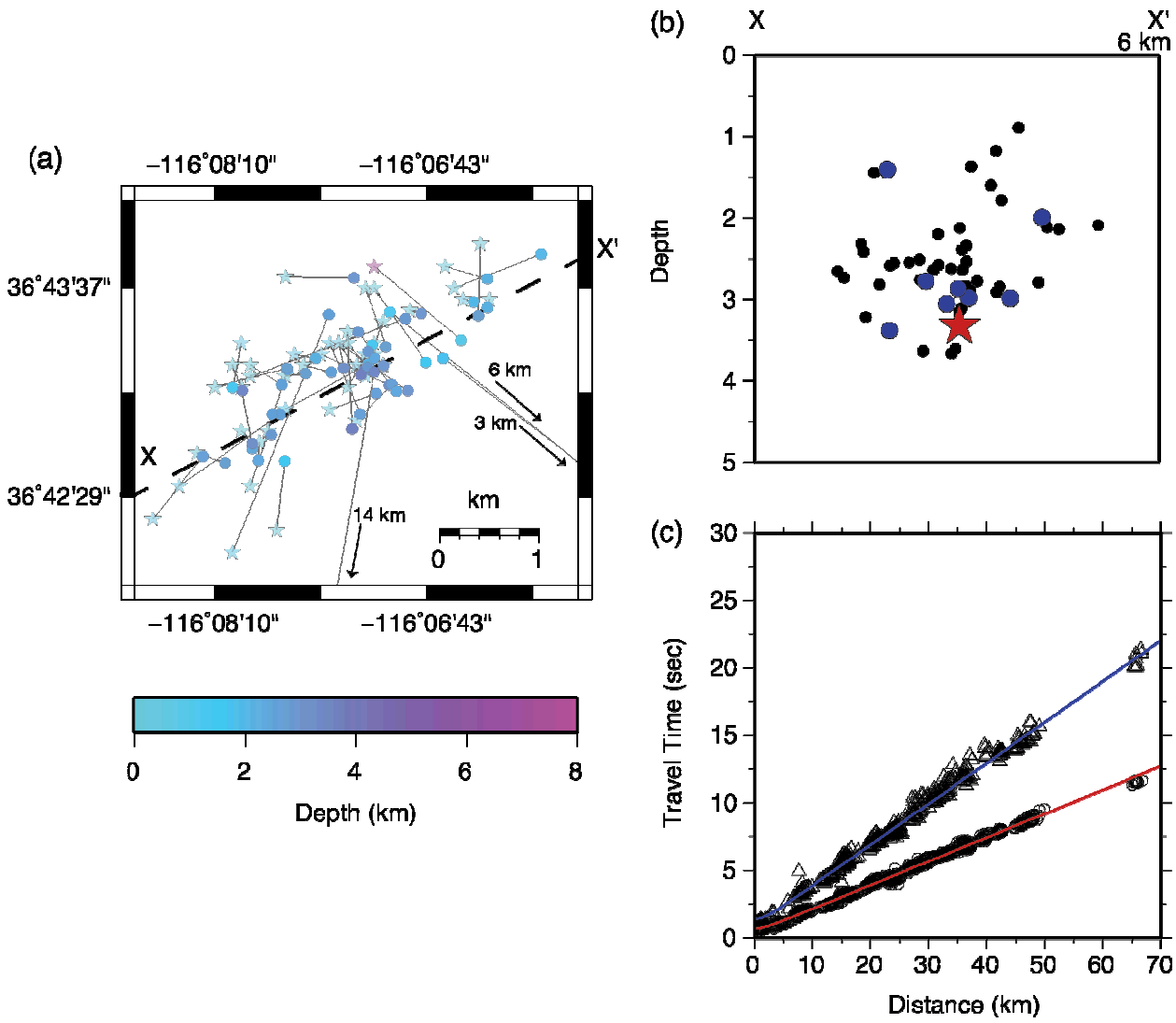

Figure 8. Direct arrival location results for Rock Valley events using the LLNL velocity model. (a) Map view of epicenter locations. Stars show the starting catalog locations for the events and circles denote the Bayesloc locations. Symbol color indicates event depth. Dashed line marks the location of the cross-section plotted in (b). Red star in (b) represents the main shock and the blue circles represent the largest aftershocks. (c) Arrival time data fits to the travel time curve at 3 km depth. Symbol and line meanings are the same as for Figure 6.

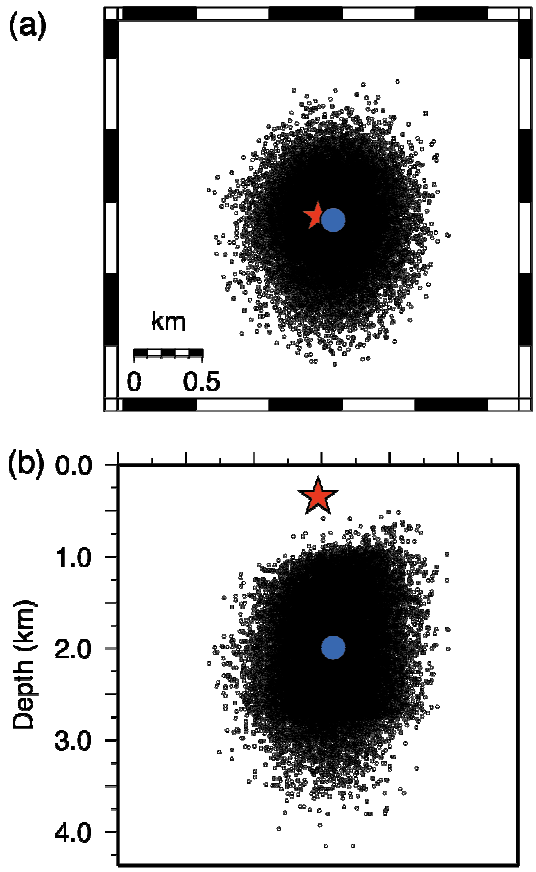

Figure 9. Example posterior distribution for one of the large Rock Valley aftershocks using the LLNL velocity model and direct arrivals only. Similar to Figure 7, except in this case the red star indicates the starting catalog location.

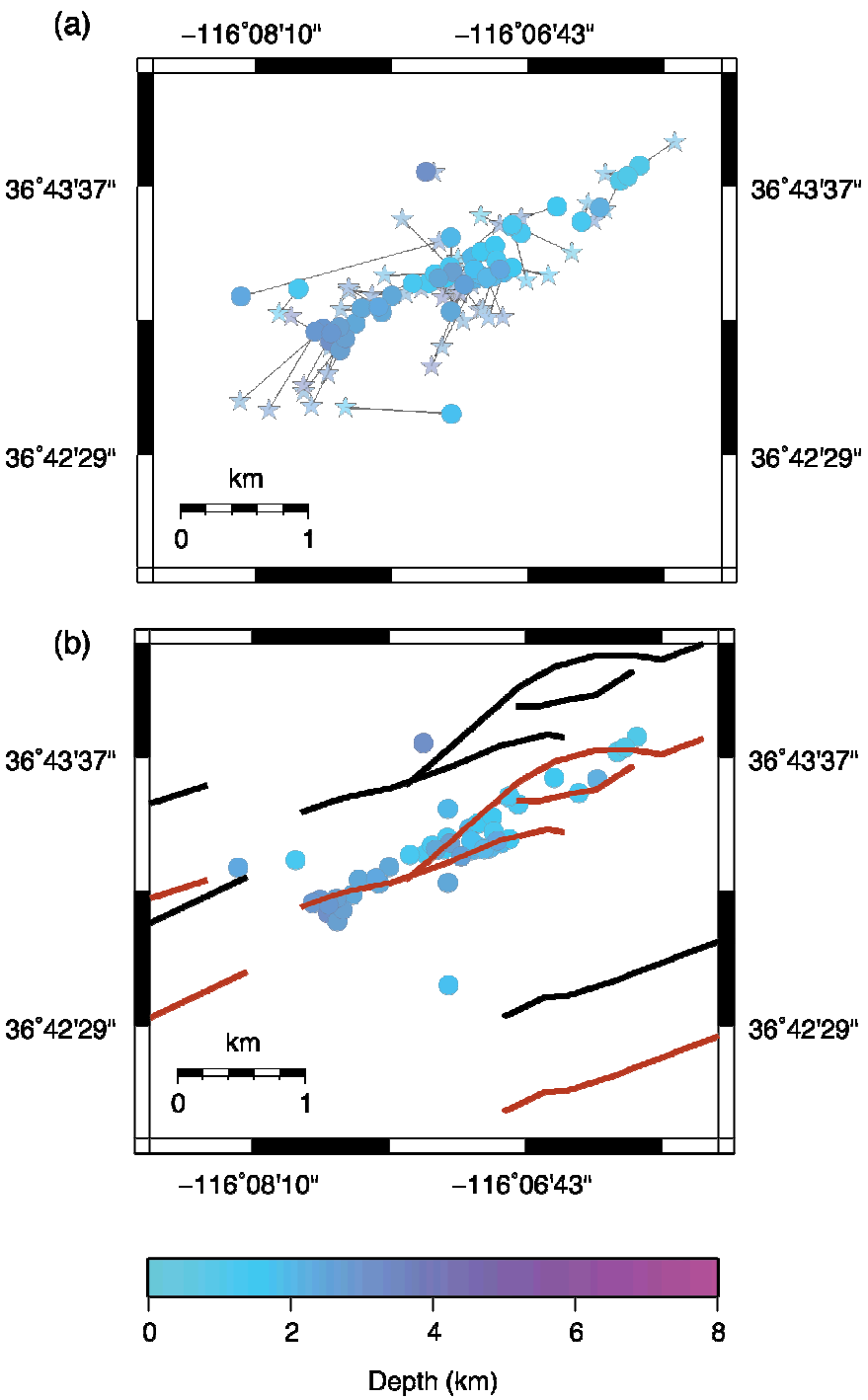

Figure 10. Direct (pick) and differential (cross correlation) arrival time location results for Rock Valley using the LLNL velocity model. (a) Comparison of results using direct arrival data only

(stars) and those using both direct and differential arrival time data (circles). (b) Event locations relative to the Rock Valley fault. Solid black lines mark the mapped fault trace (Yount *et al.*, 1987). The fault dips to the southeast (Swadley and Huckins, 1990) and red lines show the fault traces translated to the south by ~0.7 km, which could be consistent with the location of the fault at depth.

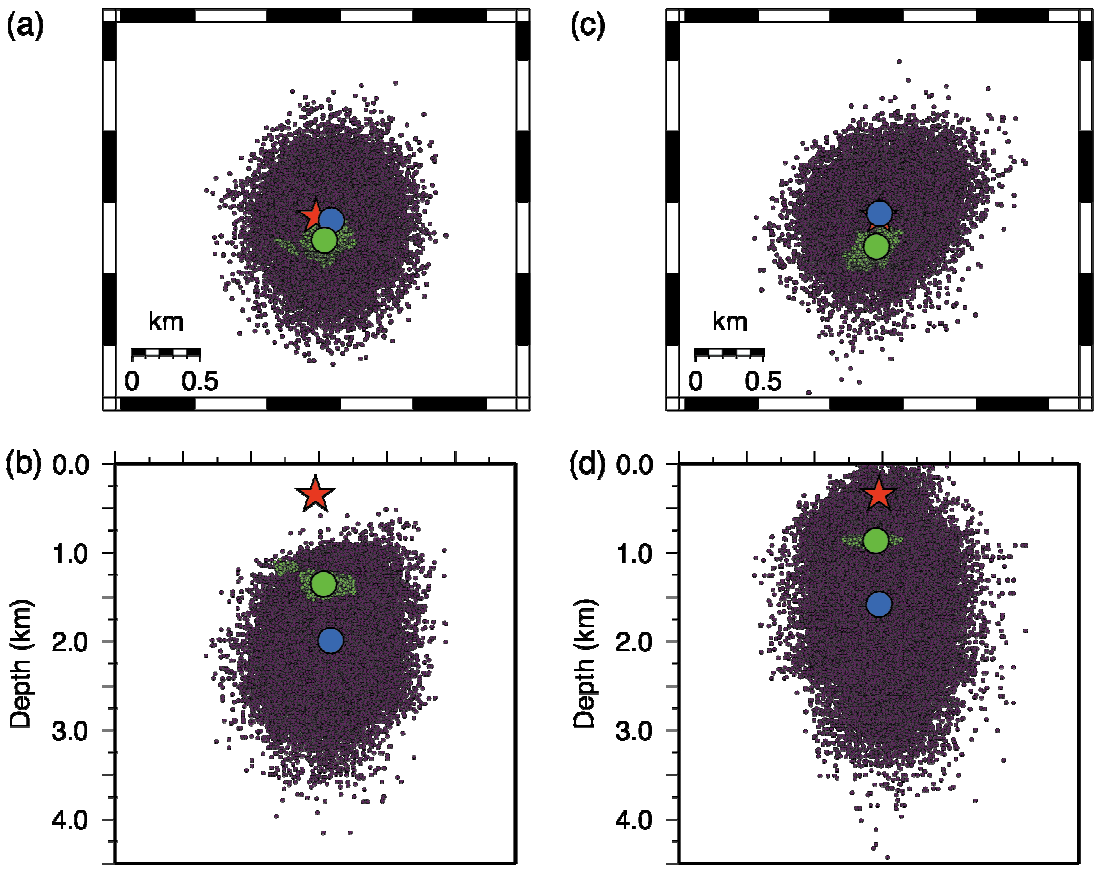

Figure 11. Comparison of posterior distributions for locations of one of the large Rock Valley aftershocks using direct arrival data only and using both direct and differential arrival time data. (a) and (b) show the map view and cross section, respectively for the LLNL velocity model and (c) and (d) show the same for the MOONHOF velocity model. In all cases the red star indicates the starting catalog location. Small dark purple circles show samples from the direct arrival posterior distribution. Large blue circle denotes the mean of the location samples based on direct arrivals. Samples from the differential and direct arrival posterior distribution are represented by small green circles, and the mean of the location samples based on direct and differential arrivals is marked by a large green circle.

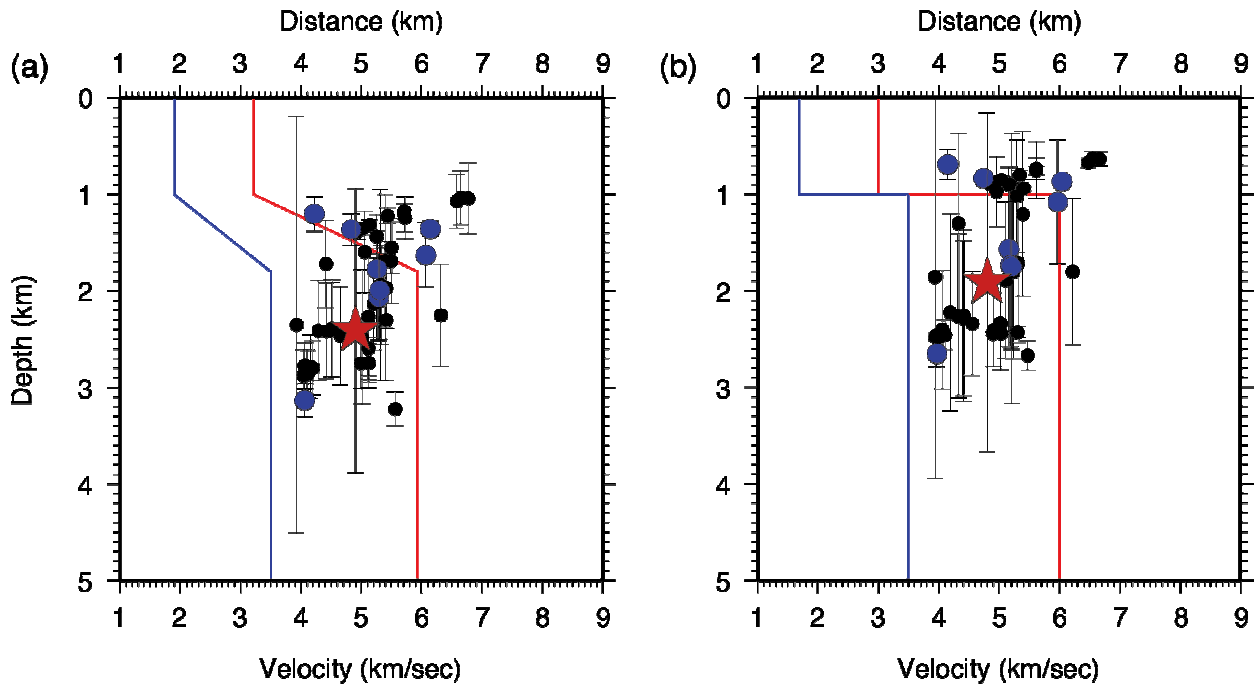

Figure 12. Cross sections showing event depths for the Rock Valley earthquakes using (a) the LLNL velocity model and (b) the MOONHOF velocity model. Red star represents the main shock and blue circles represent the largest aftershocks. Error bars indicated two standard deviations. P (red line) and S (blue line) velocity models are also plotted. Distance along the cross section is shown along the top axes while velocity is shown along the bottom axes.

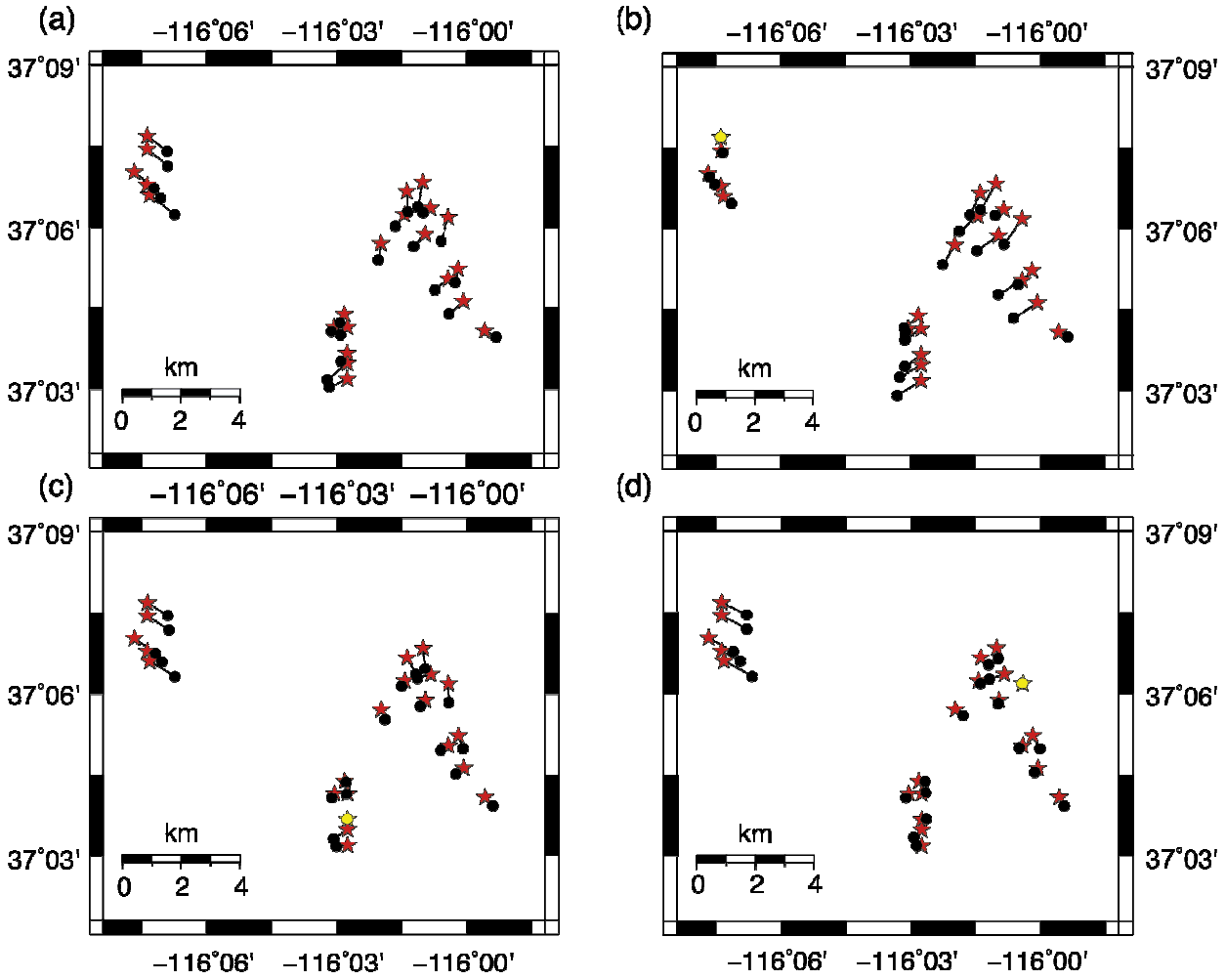

Figure 13. Nuclear test relocation results using differential arrival times and use of a tight location prior on a ground-truth event. In all cases the red stars denote true event locations, black circles show Bayesloc epicenters, and yellow symbols indicate ground-truth events constrained by a tight prior. No priors are used in (a). In cases (b), (c), and (d), a tight prior is used for a different ground-truth event each time to generate the results displayed.